

# Seismic Retrofit of Structures Using Steel Honeycomb Dampers

Minhee Lee<sup>1</sup>, Joonho Lee<sup>2</sup>, and Jinkoo Kim<sup>3\*</sup>

<sup>1</sup>Structural Engineer, Chang-Minwoo Structural Consultants, Seoul, Korea

<sup>2</sup>Structural Engineer, Metro T&C, Seoul, Korea

<sup>3</sup>Professor, Department of Civil and Architectural Engineering, Sungkyunkwan University, Suwon, Korea

## Abstract

The purpose of this paper is to investigate the seismic performance of a honeycomb shaped steel hysteretic damper applied to seismic retrofit or strengthening of a structure. The formulas for the initial stiffness and yield strength of a damper unit were derived based on the cell wall bending model, and the results were compared with those obtained from finite element analysis. Bilinear model of the honeycomb damper was developed based on the nonlinear force-displacement relationship obtained from finite element analysis. The honeycomb dampers were applied for seismic retrofit of a 15-story apartment building designed without considering seismic load and for seismic design of a 3-story moment frame designed with reduced seismic load. The analysis results showed that the honeycomb dampers were effective in the enhancement of seismic-load resisting capacity of the model structures.

**Keywords:** honeycomb, hysteretic dampers, seismic retrofit

## 1. Introduction

Hysteretic or metallic yielding dampers dissipate seismic input energy through stable hysteretic behavior and thereby contribute to enhancing seismic performance of a structure. Whittaker *et al.* (1989) and Tsai *et al.* (1993) investigated the seismic performance of steel plate added damping and stiffness (ADAS) elements and triangular plate energy absorbers (TADAS), respectively, which dissipates seismic energy through out of plane bending of steel plates. Kobori *et al.* (1992) and Benavent Climent *et al.* (1998) proposed energy-absorbing devices made of steel plates with vertical openings, which dissipates seismic energy through inplane hysteretic behavior. Chan and Albermani (2008) proposed the Steel Slit Damper (SSD) fabricated from a standard structural wide-flange section with a number of slits cut from the web, and verified its energy absorbing capacity through experiments. Benavent Climent *et al.* (2010) investigates the use of the web of standard wide-flange or I-shape sections subjected to out of plane bending as the energy-dissipating device for seismic applications. Maleki and Bagheri (2010) proposed hysteretic dampers composed

of steel pipes, filled and unfilled with concrete, and showed their effectiveness through finite element analysis and cyclic test. Maleki and Mahjoubi (2013) further developed the system into dual-pipe dampers consisting of two pipes welded at selected locations, which showed higher initial stiffness and strength. Ko *et al.* (2010) investigated the energy dissipation capacity of a wire-woven bulk Kagome damper, a kind of hysteresis damper which dissipates seismic energy through the inelastic deformation of the woven wire. Köken and Koroğlu (2015) developed a slit steel damper system for energy dissipation at beam-to-column connections of steel frames. Teruna *et al.* (2015) carried out experimental study of hysteretic steel dampers fabricated from mild steel plate with different geometrical shapes such as straight, concave, and convex shapes.

Honeycomb structure has long been applied as an efficient energy absorbing material in the field of automobile and aviation industries. Gibson and Ashby (1997) presented various formulas for hexagonal honeycomb structures such as elastic modulus, Poisson's ratio, buckling strength, etc. Wang and McDowell (2004) investigated the in-plane mechanical properties of the various periodic honeycomb structures including the Young's modulus, the elastic shear modulus, the Poisson's ratio, the yield strength in shear and the yield strength under uniaxial loading. Aref and Jung (2003) presented the polymer matrix composite (PMC)-infill wall system consisting of two fiber-reinforced polymer laminates with an infill of vinyl sheet

Received June 26, 2015; accepted September 6, 2016;  
published online March 31, 2017  
© KSSC and Springer 2017

\*Corresponding author  
Tel: +82-31-290-7563, Fax: +82-31-290-7570  
E-mail: jkim12@skku.edu

foam for seismic retrofit of structures. The experimental and analytical studies demonstrated that the introduction of a PMC-infill wall panel in a steel frame produced significant enhancements to stiffness, strength, and energy dissipation capacity. Alti-Veltin and Gandhi (2010) investigated the energy absorption capability of cellular honeycomb with various cell geometries subjected to in-plane compression through numerical analysis. Ju and Summers (2011) and Ju et al. (2012) carried out numerical studies for design of hexagonal lattice structures having a high shear strength and a high shear yield strain.

This study aimed to validate the effect of a hysteretic damper made of steel hexagonal honeycombs to enhance seismic load-resisting capacity of building structures. To this end the formulas for initial shear stiffness and yield strength of the honeycomb dampers were derived using the cell wall bending model of Gibson and Ashby (1997), which were verified by finite element analysis. The hysteretic behavior and energy dissipation capability of the dampers were also investigated. The dampers were applied for seismic retrofit of a 15-story RC moment frame not designed for seismic load, and for seismic design of a newly designed 3-story RC special moment resisting frame. The effectiveness of the dampers was verified by comparing the nonlinear dynamic analysis results of the structures without and with the dampers.

## 2. Stiffness and Strength of a Honeycomb Damper

Figure 1 depicts the configuration of a honeycomb damper installed between two floors in a building structure. The damper is expected to yield in shear and dissipates hysteretic energy when it is subjected to shear deformation due to inter-story drift during earthquake. The initial stiffness of a honeycomb damper can be obtained from the force-deformation relationship of unit honeycomb cell subjected to the shear force  $F$  shown in Fig. 2. Gibson and Ashby (1997) derived the force-

deformation relationship of a regular hexagonal cell using the wall bending model based on the assumption that there is no relative displacement of the points  $A$ ,  $B$  and  $C$  when the honeycomb is sheared. In this study the same reasoning was applied to obtain the shear stiffness and strength of a honeycomb damper. Summing moments at  $B$  gives the moment applied to the members  $AB$  and  $BC$  :

$$M = \frac{Fh}{4} \tag{1}$$

Using the standard result  $\delta = Mh^2/6EI$ , the angle of rotation is obtained as:

$$\phi = \frac{Fh^2}{24EI} \tag{2}$$

where  $E$  is the elastic modulus of the honeycomb material. The shear deflection  $u_s$  of the point  $D$  with respect to  $B$  is:

$$u_s = \frac{1}{2}\phi h + \frac{F}{3EI}\left(\frac{h}{2}\right)^3 = \frac{Fh^3}{16EI} \tag{3}$$

Using  $I = tb^3/12$ , where  $t$  is the out of plane depth of the honeycomb and  $b$  is the thickness of the cell wall, the shear force-deformation relationship can be obtained as follows:

$$F = \frac{4}{3}Et\left(\frac{b}{h}\right)^3 \cdot u_s \tag{4}$$

Figure 3 shows the analysis modeling of a unit honeycomb damper, which consists of the eight shear springs, and the shear stiffness of the unit damper can be obtained as follows:

$$\frac{1}{k_t} = \frac{2}{k_2 + 2k_3} + \frac{1}{2k_1} \tag{5a}$$

The stiffness of each spring can be obtained as follows using Eq. (4) with appropriate wall length and boundary conditions:

$$k_1 = \frac{2}{3}Et\left(\frac{b}{h}\right)^3 \tag{5b}$$

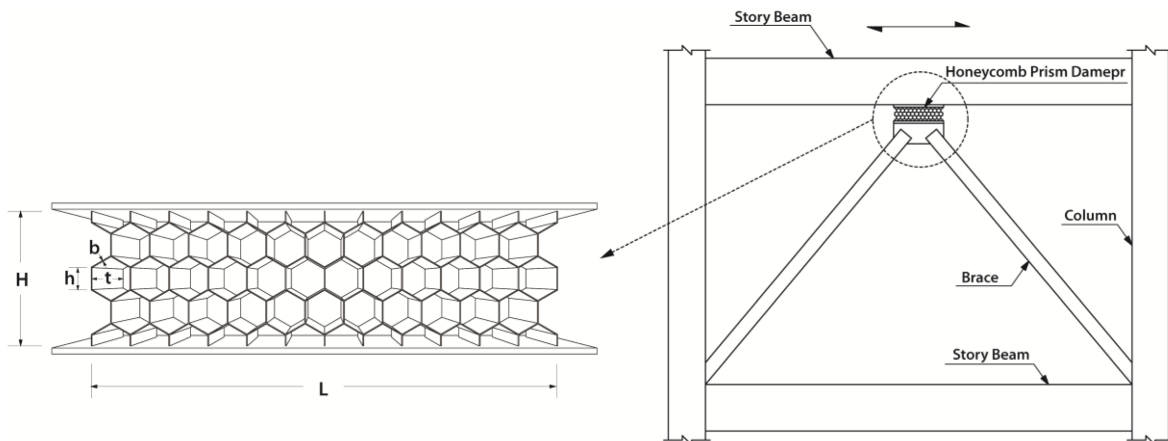


Figure 1. Configuration of honeycomb damper installed in a frame.

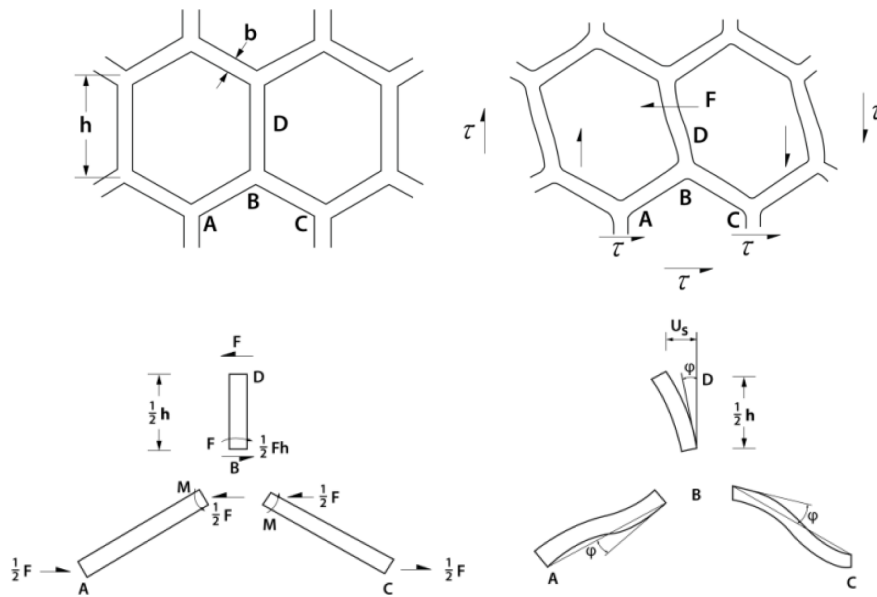


Figure 2. Cell deformation by cell wall bending and rotation (Gibson and Ashby, 1997).

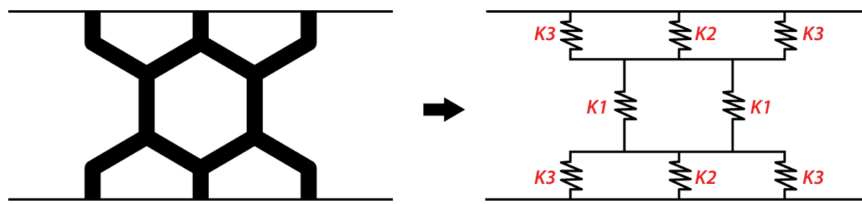


Figure 3. Analysis modeling of single honeycomb damper unit.

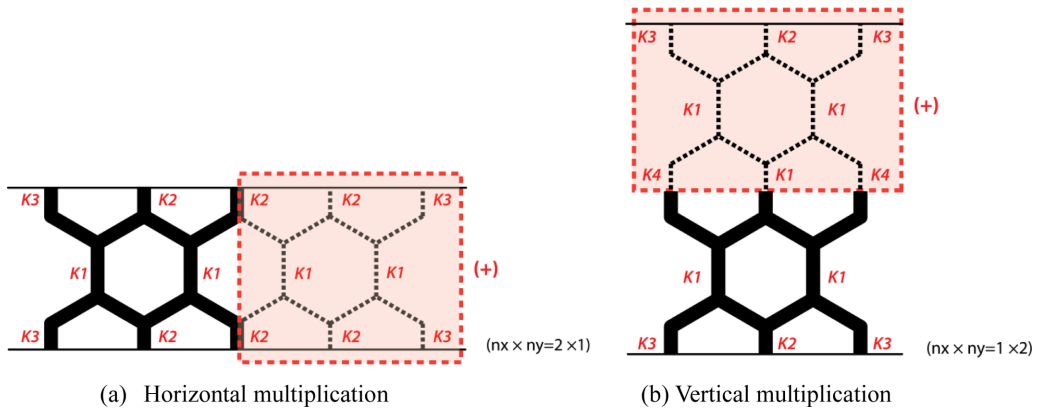


Figure 4. Honeycomb damper with multiplication of units.

$$k_2 = \frac{16}{3}Et\left(\frac{b}{h}\right)^3 \quad (5c)$$

$$k_3 = 4Et\left(\frac{b}{h}\right)^3 \quad (5d)$$

Figure 4 shows the horizontal and vertical multiplications of the unit damper. When  $n_x$  units of dampers are added horizontally to the unit damper, the stiffness of the damper becomes as follows:

$$\frac{1}{k_t} = \frac{2}{(2n_x - 1)k_2 + 2k_3} + \frac{1}{2n_x k_1} \quad (6a)$$

When  $n_y$  units are added vertically, the shear stiffness can be obtained as

$$\frac{1}{k_t} = \frac{2}{(2n_x - 1)k_2 + 2k_3} + \frac{n_y}{2n_x k_1} + \frac{n_y - 1}{(2n_x - 1)k_1 + 2k_4} \quad (6b)$$

The shear stiffness increases with horizontal extension of the unit system and decreases with vertical extension

of the system. In case there are  $n_x$  units of honeycomb dampers horizontally and  $n_y$  units vertically, the overall stiffness can be obtained as follows:

$$\frac{1}{k_t} = \frac{2}{(2n_x-1)k_2+2k_3} + \frac{n_y}{2n_x k_1} + \frac{n_y-1}{(2n_x-1)k_1+2k_4} \quad (6c)$$

$$k_t = \frac{4n_x(4n_x+1)}{3\{(8n_y-3)n_x+n_y\}} Et \left(\frac{b}{h}\right)^3 \quad (6d)$$

It can be observed in Eq. (6) that the thickness-to-height ratio ( $b/h$ ) of the cell wall is an important parameter for the stiffness of the honeycomb damper.

Figure 5 shows the shear force distribution in each cell wall of a unit honeycomb damper. In case there are  $n_x$  unit dampers along the horizontal line, the horizontal shear force acting on each cell wall at the mid-height is  $V/2n_x$ , and the bending moment and the maximum stress at the end of the vertical cell wall are as follows:

$$M = \frac{hV}{4n_x} \quad (7a)$$

$$\sigma = \frac{My}{I} = \frac{hV}{4n_x} \times \frac{b}{2} \times \frac{12}{tb^3} = \frac{3hV}{2n_x tb^2} \quad (7b)$$

The shear strength at complete yielding of the cross section can be obtained from multiplying the shear strength at yield,  $V_{yo}$ , obtained from Eq. 7(b) with the shape factor for a rectangular section, which is 1.5:

$$V_{y,t} = 1.5V_{yo} = \frac{n_x \sigma_y t b^2}{h} \quad (8)$$

where  $\sigma_y$  is the first yield stress of the material. The yield displacement  $\Delta_{y,t}$  can be obtained by dividing  $V_{y,t}$  with the stiffness  $k_t$  computed previously:

$$\Delta_{y,t} = \frac{V_y}{k_t} = \frac{3\{(8n_y-3)n_x+n_y\} \sigma_y h^2}{4(4n_x+1)E_s b} \quad (9)$$

### 3. Finite Element analysis of a Damper Unit

The equations derived above can predict only the elastic behavior of the honeycomb damper in small displacement. To observe complete behavior of the damper up to failure, finite element analysis was carried out using the program code ABAQUS. Total of 12 honeycomb damper models

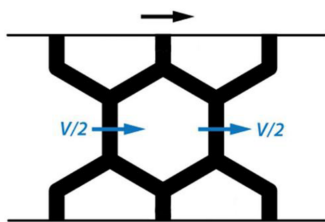


**Figure 5.** Shear force distribution in each wall of unit honeycomb damper subjected to shear force  $V$ .

**Table 1.** Dimensions of models (units: mm)

Model	L	H	t	h	b	b/h	No. of cells ( $n_x \times n_y$ )
HD-1	520	150	100	25	2	0.08	6×2
HD-2	-	-	-	-	2.25	0.09	-
HD-3	-	-	-	-	2.5	0.1	-
HD-4	-	-	-	-	2.75	0.11	-
HD-5	-	-	-	-	3	0.12	-
HD-6	-	-	-	-	3.25	0.13	-
HD-7	514	148.5	100	16.5	1.3	0.079	9×3
HD-8	-	-	-	-	1.5	0.091	-
HD-9	-	-	-	-	1.65	0.1	-
HD-10	-	-	-	-	1.8	0.109	-
HD-11	-	-	-	-	2	0.121	-
HD-12	-	-	-	-	2.15	0.13	-

with different cell sizes and  $b/h$  ratios were prepared for analysis, and the dimension of each model is presented in Table 1, where  $L$  and  $H$  denote the overall horizontal and vertical dimensions of the model, respectively,  $t$  is the depth of the honeycomb, and  $b$  and  $h$  are the thickness and the height of the vertical cell wall, respectively. The  $b/h$  ratio, which is considered to be the most important design parameter, was varied from 0.08 to 0.13 at the interval of 0.01. The heights of the vertical cell walls are 16.5 and 25 mm.

The dampers are made of mild steel with yield and ultimate strengths of 330 and 510 N/mm<sup>2</sup>, respectively. Figure 6 shows the stress-strain curve of the material used, and Fig. 7 depicts the analysis model with rigid plates attached to the top and bottom of the damper. Monotonically increasing horizontal shear force was enforced at the top and bottom rigid plates. Both the material and the geometric nonlinearities were considered in the analysis. Shell elements (S4R) were chosen to model the damper based on the fact that the thickness of

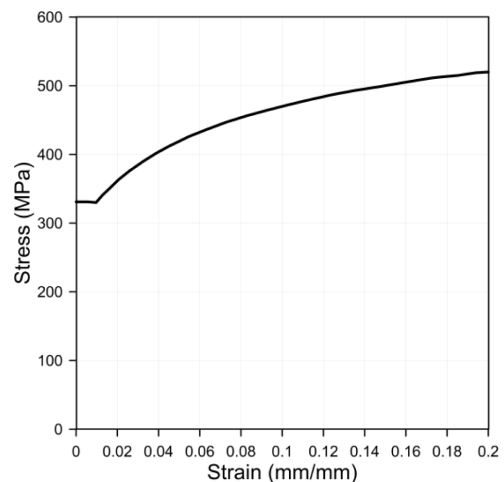


**Figure 6.** Stress-strain curve of the structural steel.

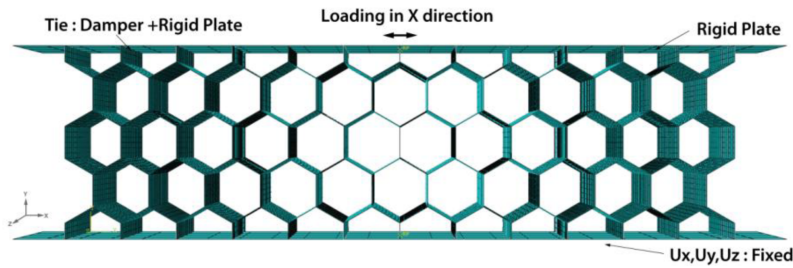


Figure 7. Boundary conditions of the honeycomb damper (HPD-1).

the cell wall is significantly smaller than the other dimensions. In addition solid elements (C3D8R\_8-node brick, and C3D20R\_20-node brick) with 8 and 20 nodes were also used to model the damper for comparison. Shell elements are generally used to model structural elements in which two dimensions are much greater than the third one. In this case the solid element tends to show stiffer bending behavior due to locking phenomenon. The force-displacement relationships of the damper HD-1 obtained from three different finite element modeling are plotted in Fig. 8, where it can be observed that after the first yield the strength keeps increasing due to strain hardening, and the rate of increase in strength becomes higher in large displacement as a diagonal tension strut is formed across the cells. The analysis results obtained from the three different finite element models are similar in the elastic regime; however as the deformation increases the strengths obtained using the solid elements become higher than the strength obtained using the shell elements. Based on the analysis results the shell elements, which provided the most conservative force-deformation relationship, were used to model the honeycomb damper.

Figure 9 shows the force-displacement relationships of the twelve analysis models plotted up to the maximum strain of 0.2 (displacement of 30 cm). It was observed that the vertical cell walls yielded first followed by the yielding of the slanted cell walls. It can be noticed in the figure that both stiffness and strength increase as the thickness-to-height ratio ( $b/h$ ) of the cell wall increases. As  $b/h$  ratio increased by 0.01 the stiffness and the

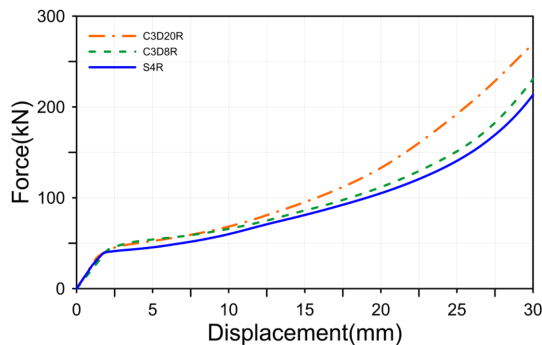


Figure 8. Comparison of the shear force-displacement relationship of the honeycomb damper (HD-1) modeled with shell and solid elements.

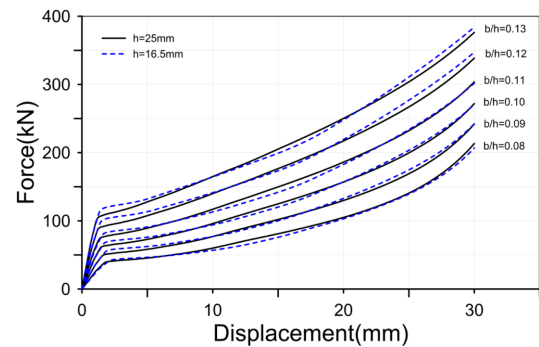


Figure 9. Force-displacement curve of the honeycomb damper with different cell height.

strength of the damper increased by 33% and 21% in average, respectively. For the same  $b/h$  ratio the difference in the height of the cell wall did not make significant change in the stiffness and the strength as can be observed in the results of the models HD-1 and HD-7, HD-2 and HD-8, etc. Figure 10 depicts the von Mises stress contour of the damper HD-1 and HD-7 at the lateral displacement of 30 mm. It can be observed that high stress is induced at the cell wall joints, especially along the tension field formed diagonally from the left bottom end to the right top end of the dampers.

Table 2 compares the stiffness and the strength of the analysis models obtained from the FE analysis and the formulas given in Eq. (6) and Eq. (8), respectively. The comparison shows that the differences in the initial stiffness and the shear yield strength range from 1 to 8% and 7 to 22%, respectively. The relatively large difference in the prediction of the shear yield strength can also be observed in the study of Ju *et al.* (2012), who attributed the difference to the fact that the simplified modeling of the shear strength of a honeycomb cell provided by the Gibson and Ashby (1997) fails to cover the local micro-rotation of cell walls, which induces more local stresses, resulting in a lower strain.

To investigate the hysteretic behavior of the damper, cyclic analyses of the model HD-1 to HD-4 were carried out using the loading protocol for quasi-static cyclic testing recommended in the FEMA 461 (2007) and shown in Fig. 11. The target displacement was set to be 30 mm which corresponds to 1% of the story height of a typical

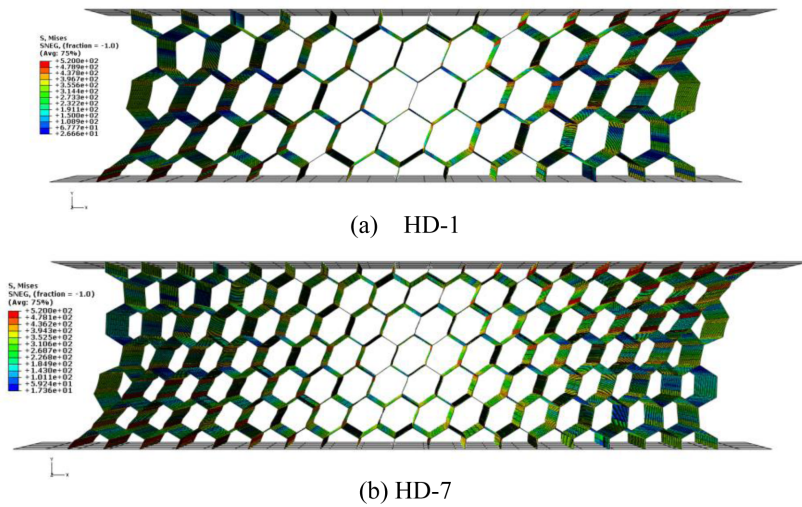


Figure 10. von Mises stress contour of the FE model at lateral displacement of 30 mm.

Table 2. Comparison of analysis results for monotonic load obtained from the FE analysis and the formulas

Model	k (kN/mm)	$k_t$ (kN/mm)	$k/k_t$	$V_y$ (kN)	$V_{y,t}$ (kN)	$V_y/V_{y,t}$	$\Delta_y$ (mm)	$V(@\Delta = 30 \text{ mm})$ (kN)
HD-1	24.92	25.60	0.97	26.83	31.78	0.84	1.09	213.37
HD-2	35.18	36.45	0.97	33.06	40.22	0.82	0.94	242.05
HD-3	47.81	50.00	0.96	41.55	49.65	0.84	0.88	271.95
HD-4	62.99	66.55	0.95	49.69	60.08	0.83	0.79	303.78
HD-5	80.87	86.40	0.94	60.49	71.50	0.85	0.76	338.68
HD-6	101.61	109.85	0.92	65.36	83.91	0.78	0.64	376.35
HD-7	22.98	22.62	1.02	28.21	30.51	0.92	1.24	206.80
HD-8	34.94	34.75	1.01	32.99	40.62	0.81	0.94	242.18
HD-9	46.11	46.25	1.00	44.41	49.15	0.90	0.97	270.82
HD-10	59.31	60.05	0.99	47.07	58.50	0.80	0.79	302.02
HD-11	80.28	82.37	0.97	63.66	72.22	0.88	0.79	347.42
HD-12	98.66	102.32	0.96	77.52	83.46	0.93	0.79	384.17

apartment building (3m). Figure 12 depicts the hysteresis curves of the model HD-1 and HD-4, where it can be noticed that all dampers show stable hysteresis curves. The area enclosed in the curve, which indicates the dissipated hysteretic energy, increases as the  $b/h$  ratio increases. Figure 13 shows that the dissipated energy increases as the cumulative displacement and  $b/h$  ratio increase.

The effective viscous damping ratio of the damper,  $\zeta_{eff}$ , can be estimated using the following simple formula (Chopra 2007):

$$\zeta_{eff} = \frac{1}{4\pi} \frac{E_D}{E_{s0}} \tag{10}$$

where  $E_{s0}$  is the potential energy stored at the maximum displacement  $\delta_{max}$  and  $E_D$  is the dissipated energy during one cycle of vibration.  $E_{s0}$  is obtained by  $1/2k_{eff}\delta_{max}$ , where  $k_{eff}$  is the effective stiffness at the maximum displacement, and  $E_D$  is the area of the hysteresis curve. Figure 14 shows the relationships between the effective

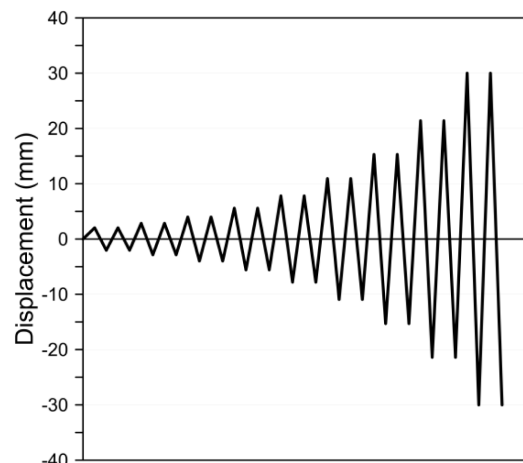


Figure 11. Displacement loading history specified in FEMA 461.

damping ratio and the normalized stiffness,  $k_{eff}/k_t$ , at various loading cycles, where  $k_t$  is the initial stiffness. It

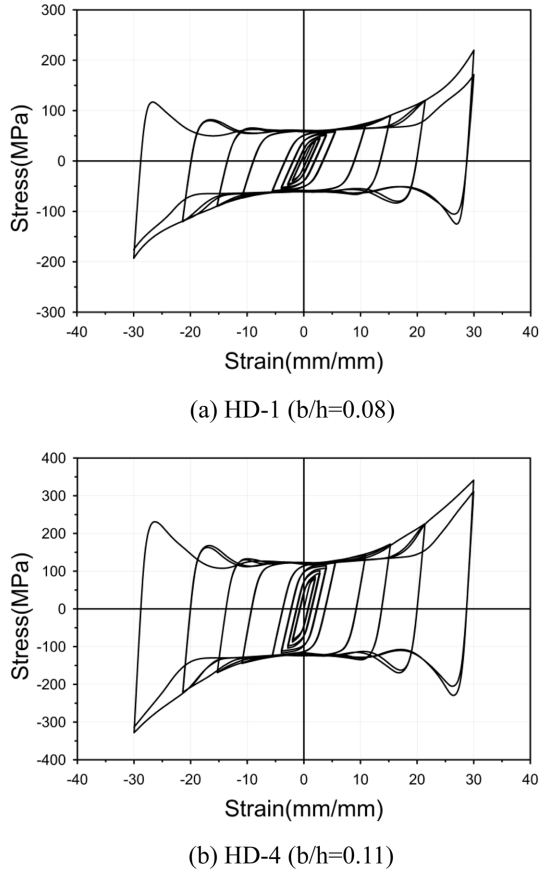


Figure 12. Hysteresis diagram of the honeycomb dampers.

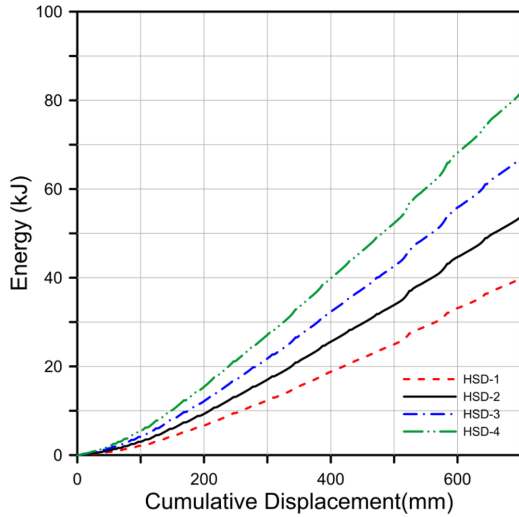


Figure 13. Cumulative dissipated energy of the honeycomb dampers.

can be observed that the effective damping ratio of the honeycomb dampers ranges from 37 to 51%, and generally decreases as the effective stiffness increases. This result is similar to the result observed in the tests of steel slit dampers (Chan and Albermani, 2007).

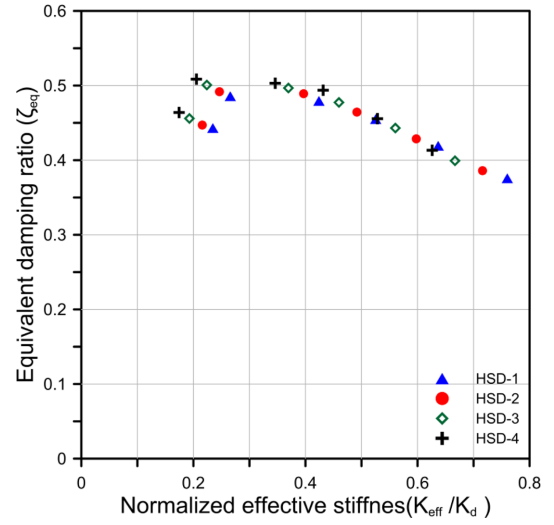


Figure 14. Equivalent damping ratio of the honeycomb dampers.

#### 4. Bilinear Idealization of the Honeycomb Damper

For seismic retrofit of a structure using the honeycomb damper, a series of nonlinear dynamic analysis using various earthquake records is generally required. To save the computation time required for dynamic analysis of a nonlinear system, the nonlinear force-displacement relationship of the damper unit was idealized as bilinear lines in such a way that the areas under the actual and the idealized curves are identical as shown in Fig. 15. The yield point of the bilinear curve,  $E$ , was determined as the cross point of the initial stiffness line and the tangent line at the starting point of the strain hardening,  $D$ . The maximum displacement was set to be 20% of the total damper height, and the strength at the maximum displacement,  $H$ , corresponds to the effective maximum strength of the idealized system. Table 3 shows the parameters required to transform the nonlinear model for each damper into the bilinear model, such as the ratio of the initial stiffness ( $\alpha_1 = k/k_t$ ), strength ratio ( $\beta_1 = V_p/V_{y,t}$ ,  $\beta_2 = V_u/V_{y,t}$ ), and the stiffness ratio after yield ( $\gamma_1 = k_p/k_t$ ), where  $k$  is the initial stiffness obtained from FE analysis,  $V_p$  and  $V_u$  are the yield and the ultimate force obtained from the equivalent bilinear model, and  $k_t$  and  $V_{y,t}$  are the initial stiffness and the yield strength obtained from the formulas Eq. (6) and Eq. (8), respectively. Using those parameters the post-yield stiffness and the strength of the simplified bi-linear model can be defined as follows:

$$k = \alpha_1 k_t \quad (11)$$

$$V_p = \beta_1 V_{y,t} \quad (12)$$

$$\Delta_p = \frac{\beta_1}{\alpha_1} \Delta_{y,t} \quad (13)$$

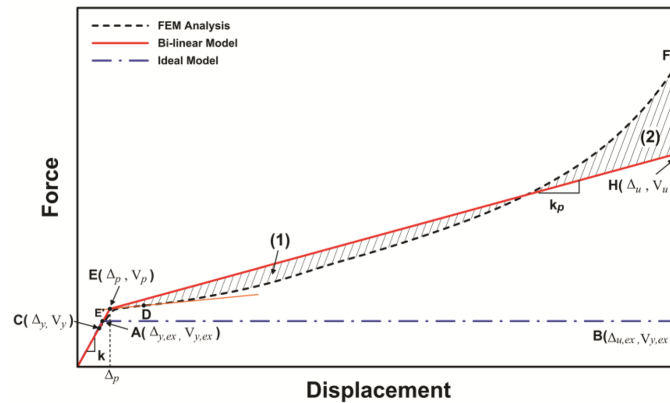


Figure 15. Bi-linearized stress-strain curve.

Table 3. Results of a simplified bi-linear stress-strain curve

Model	$V_p$ (kN)	$V_p/V_{y,t}$	$V_u$ (kN)	$V_u/V_{y,t}$	$K_p$ (kN/mm)	$k_p/k$
HD-1	40.32	1.27	148.88	4.69	3.82	0.15
HD-2	50.79	1.26	180.20	4.48	4.53	0.13
HD-3	63.13	1.27	213.20	4.29	5.23	0.11
HD-4	75.81	1.26	249.65	4.16	6.04	0.10
HD-5	89.16	1.25	289.84	4.05	6.94	0.09
HD-6	105.05	1.25	330.54	3.94	7.78	0.08
HD-7	43.17	1.41	142.48	4.67	3.53	0.15
HD-8	57.06	1.40	178.97	4.41	4.30	0.12
HD-9	69.73	1.42	208.50	4.24	4.87	0.11
HD-10	82.68	1.41	240.63	4.11	5.52	0.09
HD-11	102.29	1.42	286.46	3.97	6.41	0.08
HD-12	118.23	1.42	322.54	3.86	7.09	0.07
average		1.34 ( $\beta_1$ )		4.24 ( $\beta_2$ )		0.11 ( $\gamma_1$ )

$$k_p = \gamma_1 \alpha_1 k_t \quad (14)$$

$$V_u = \beta_2 V_{y,t} \quad (15)$$

where the yield displacement  $\Delta_{y,t}$  is obtained from Eq. (9), and the mean values of the parameters  $\alpha_1$ ,  $\beta_1$ ,  $\beta_2$ , are  $\gamma_1$  are 0.97, 1.34, 4.24, and 0.11, respectively.

## 5. Seismic Retrofit of a 15-story Structure with Honeycomb Dampers

### 5.1. Analysis modeling of the case study structure

The effectiveness of the honeycomb dampers was verified through the analysis of a 15-story reinforced concrete apartment building before and after the retrofit. Figure 16 shows the configuration and dimension of the analysis model structure, which has the typical plan shape of apartment buildings built during early 1970's in Korea. The structure was designed to resist wind load as well as gravity loads, but earthquake load was not considered in the design. Therefore longer sides of columns are located

along the transverse direction which is subjected to larger wind load. The slabs were assumed to be rigid diaphragm, and the strengths of reinforced concrete and re-bars were assumed to be 21 MPa and 400 MPa, respectively. The columns and beams in three consecutive stories were designed using the same elements. Considering the low story height, the depth of floor beams was limited to 35 cm. The dimensions and re-bar placements of the structural elements in the first story are shown in Table 4. The effective stiffness of the beams and columns in elastic range was reduced to  $0.5E_cI_g$  and  $0.7E_cI_g$ , respectively, considering cracked section. The shear strength of the elements was reduced to  $0.4E_cA_v$ . The fundamental natural period of the model structure turned out to be 2.7 second along the longitudinal direction and 2.3 second along the transverse direction. Inherent damping ratio of 5% of the critical damping was assumed in the dynamic analysis.

For nonlinear analysis, the beams and columns were modeled by beam and column elements in Perofom 3D, respectively, and their nonlinear bending moment vs. rotation relationships of represented by tri-linear lines as shown in Fig. 17. The post yield stiffness varies depending on the axial force as specified in the ASCE/SEI 41-06. Following the recommendation of ASCE/SEI 41-06, the over-strength factors of 1.5 and 1.25 were applied for the strength of reinforced concrete and re-bars, respectively.

### 5.2. Seismic performance of the model structure

The seismic performance of the model structure was evaluated using the seismic performance criteria of ASCE/SEI 41 (2006). Nonlinear static analysis was carried out using the program code Perform 3D (2006). Pushover analyses were carried out along the longitudinal and the transverse directions using a lateral load proportional to the fundamental mode shape in each direction. Monotonically increasing lateral loads were applied until the roof displacements reached 4% of the building height, and the base shear vs. roof displacement curves were plotted in Fig. 18. The p-delta effect option was selected in the analysis, and the gravity load of 1.1 DL + 0.25 LL was

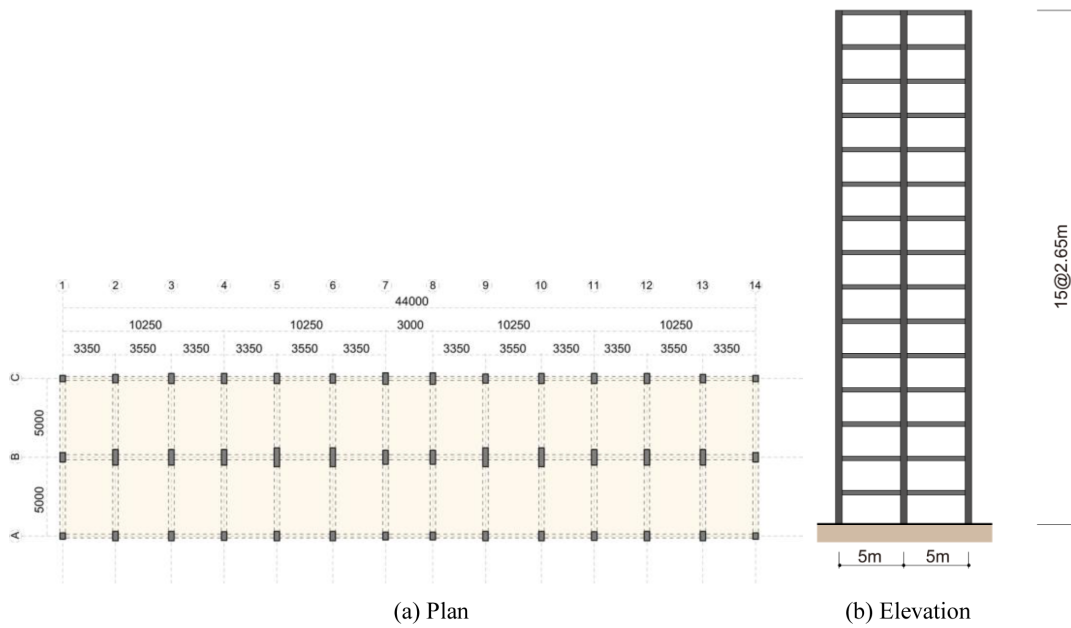


Figure 16. Configuration of the analysis model structure.

Table 4. Size of the first story beams and columns (mm)

(a) Beams			
Name	Beam size (width×depth)	Rebar	
		Ends	Middle
GA	250×250	2-D16	2-D16
GB	330×300	2-D19	2-D19
GC	250×250	2-D16	2-D16
G1	330×350	4-D22	2-D22
G2-6	350×350	6-D22	4-D22
G7	330×350	6-D22	2-D22

(b) Columns			
Name	Column size	Rebar	
		Main	Tie
CA1	350×400	8-3 D19	D10@250
CA2-3	350×600	8-3 D29	D10@400
CA4	350×550	8-3 D25	D10@400
CA5-6	350×600	8-3 D29	D10@230
CA7	350×500	8-3 D25	D10@400
CB1	350×600	8-3 D25	D10@370
CB2-3	350×1000	12-3 D29	D10@210
CB4	350×1000	12-3 D29	D10@210
CB5-6	350×1200	12-3 D32	D10@400
CB7	350×900	12-3 D29	D10@400

imposed on the structure for seismic analysis. The points corresponding to the design base shear, yield point, and the maximum inter-story drift of 2% were indicated on the pushover curves. The design base shears were obtained using the response spectral acceleration recommended by the current seismic design code of Korea, the design spectral

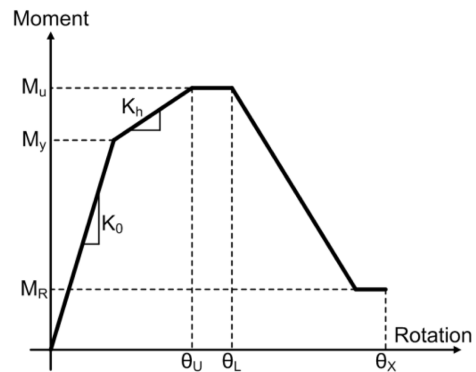


Figure 17. Nonlinear moment-rotation relationship of bending members.

acceleration coefficients  $S_{DS} = 0.49$  and  $S_{D1} = 0.28$ . The response modification factor of 3.0 and the importance factor of 1.2 were also used. It can be observed in the pushover curves that the strength along the longitudinal direction is significantly smaller than the strength along the transverse direction, even smaller than the design base shear required by the current design code. This is due to the fact that the design wind load along the transverse direction is much higher, and the seismic load was not considered in the design. It was observed that, when loaded along the longitudinal direction, plastic hinges first formed at the beams in the mid height and subsequently spread throughout the stories. The strength rapidly decreased when plastic hinges formed at the columns in the tenth and eleventh stories. Based on the pushover analysis results it was concluded that the model structure needed seismic retrofit along the longitudinal direction to resist the seismic load required by current design code.

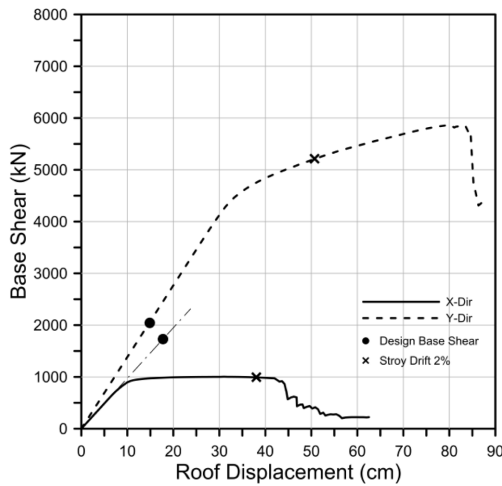


Figure 18. Pushover curves of the model structure.

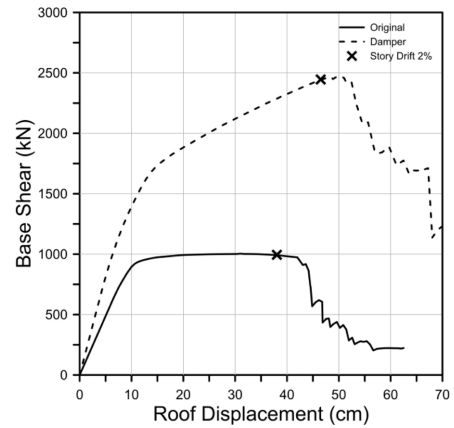


Figure 20. Pushover curves of the model structure before and after retrofit with honeycomb dampers.

**5.3. Response of the structure retrofitted with honeycomb dampers**

For seismic retrofit of the analysis model structure, two honeycomb dampers were installed per story in the center frame (frame B in Fig. 16) along the longitudinal direction as depicted in Fig. 19. Dampers were installed between two floors using the rigid chevron bracing from 2<sup>nd</sup> to 9<sup>th</sup> story where inter-story drifts are relatively large. Based on some trials, it was confirmed that the strength of the retrofitted structure satisfied the design base shear when the shear capacity of the dampers installed in each story was 27.5% of the design base shear, which is 475 kN. The dimension of the damper was determined so that the maximum shear strain of 0.2 was reached at the inter-story drift of 1.5% of the story height. The total width and height of the damper were determined to be 1,067 mm and 198 mm, respectively, and the height and the thickness of

each cell wall are 22 mm and 2.9 mm, respectively. The depth of the damper was determined as 100 mm. Using Eq. (11) to (15) the initial and the post-yield stiffness are computed as 159.19 and 17.51 kN/mm, respectively, and the yield and ultimate strength are 237.37 and 751.10 kN, respectively.

The bi-linear behavior of the honeycomb damper was modeled using the ‘Rubber Type Seismic Isolator Element’ in the Perform 3D. Figure 20 shows the pushover curves of the structure along the longitudinal direction before and after the retrofit. It can be observed that both stiffness and strength of the model structure increased significantly as a result of the damper installation. It was observed that plastic hinges first formed at the middle story beams and spread to the beams in the nearby stories, as observed in the structure before retrofit.

Nonlinear dynamic analyses were carried out using the

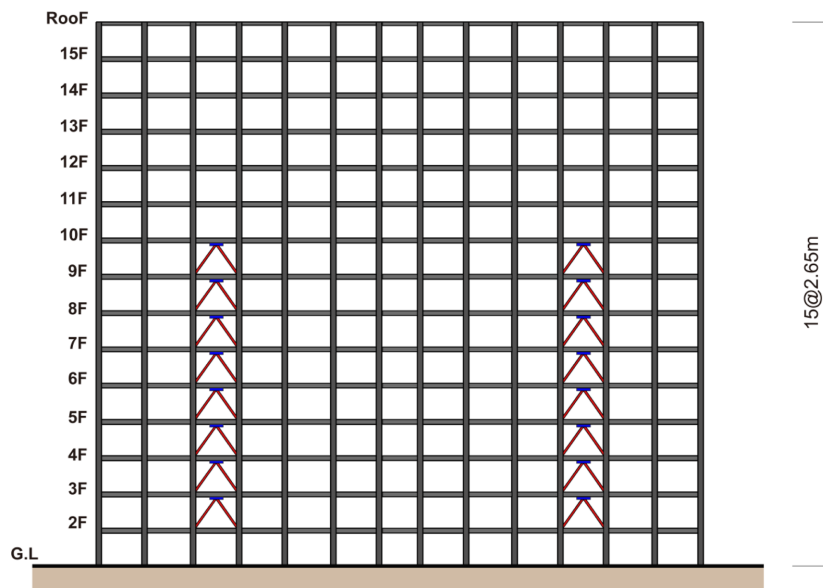
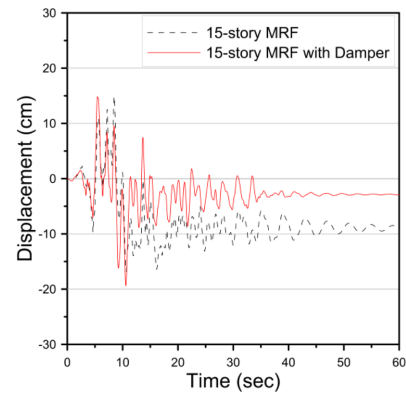


Figure 19. Location of honeycomb dampers in the 15-story structure.

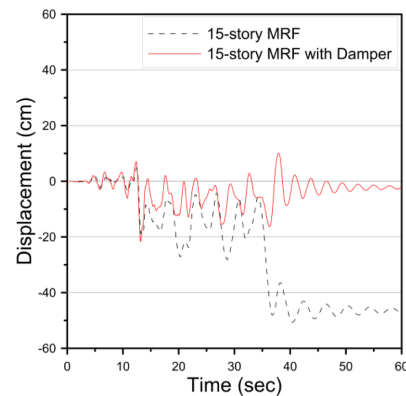
**Table 5.** Earthquake records used in dynamic analysis

ID	Name	Component	PGA (g)
1C1	Northridge (1994)	NORTHR/MUL009	0.52
5C1	Imperial Valley (1979)	IMPVALL/H-DLT262	0.35
7C1	Kobe (1995)	KOBE/MIS000	0.51
13C1	Loma Prieta (1989)	LOMAP/CAP000	0.53
16C1	Superstition Hills (1987)	SUPERST/B-ICC000	0.36
19C1	Chi-Chi (1999)	CHICHI/CHY101-E	0.44
21C1	San Fernando (1971)	SFERN/PEL090	0.21

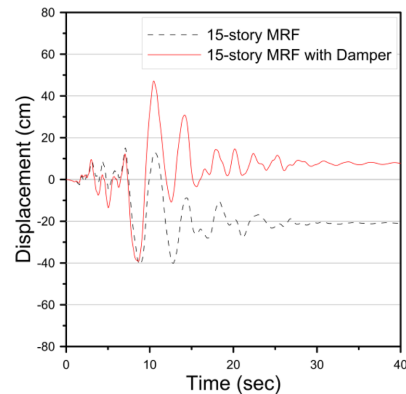
seven earthquake records provided in the Pacific Earthquake Engineering Research (PEER) Center NGA Database. The characteristics of the records are presented in Table 5. The records were scaled in such a way that the response spectral acceleration of each record corresponding to the natural period of the structure matches with the design spectrum. Figure 21 shows the time histories of the top story displacements of the structure before and after the retrofit obtained from the analysis. It can be observed that in most cases both the maximum displacement and the permanent displacement decreased due to the installation of the dampers. Figure 22 depicts the hysteresis curve of the damper located in the second story during Kobe earthquake, where it can be observed that the dampers experienced many cycles of full yielding, dissipating large amount of seismic energy. Compared with the hysteretic behavior of the damper obtained from the FE analysis presented in Fig. 12, the hysteresis curve shown in Fig. 22, which was obtained based on the simplified bilinear stress-strain relationship, has higher unloading stiffness. This may lead to smaller residual displacement in the model structure installed with the dampers than actually occurs in the structure. Therefore the significant reduction in the permanent displacement observed in Fig. 21 may be partly contributed from the bilinear simplification of the hysteretic behavior. Figure 23 shows the maximum inter-story drifts of the model structure obtained from nonlinear dynamic analysis before and after the retrofit. Before the retrofit the inter-story drifts obtained from some records exceeded the limit state of 2% of the story height, whereas in the retrofitted structure all inter-story drifts are within the limit state. The reduction of inter-story drifts is most significant in the stories where dampers are installed. The reduction in the inter-story drift seems to be contributed from the installation of the dampers, not from the change in the natural period of the structure, based on the observation that the seismic demand generally increases as a result of decrease in natural period after dampers are installed. The dissipated energy in the structure during each earthquake is plotted in Fig. 24. It can be observed that seismic energy was dissipated in the beams of the structure without retrofit, whereas in the structure with honeycomb dampers



(a) Loma Prieta



(b) Superstition Hills



(c) San Fernando

**Figure 21.** Nonlinear dynamic analysis results of the model structure for various earthquake records before and after retrofit.

significant amount of energy was dissipated in the dampers and the energy dissipated by the beams was greatly reduced. This implies that less damage occurred in the structural members.

## 6. Seismic Design of a New Moment framed Structure with Honeycomb Dampers

In this section the honeycomb dampers were applied to seismic design of a three-story RC moment frame located

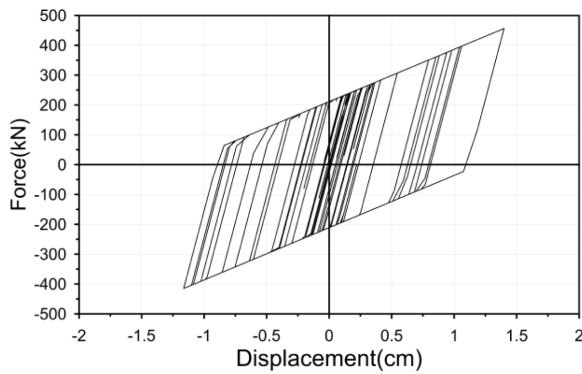


**Figure 22.** Hysteresis loop of the 2<sup>nd</sup> story honeycomb damper subjected to Kobe EQ.

in downtown Los Angeles. The building was designed per ASCE 7-10 as a special moment frame using the design spectral acceleration coefficients  $S_{DS} = 0.73$  and  $S_{D1} = 0.60$  with site coefficients for the Stiff Soil. The ultimate strengths of concrete and reinforcing steel are 27 MPa and 400 MPa, respectively. Figure 25(a) shows the structural plan and elevation of the model structure.

The perimeter special moment frames were designed to resist all seismic load and the interior frames were designed only for gravity load. Table 6 shows the member size and re-bar placement of the model structure, where GB and GC represent the interior beams and columns, respectively, and SB1 and SC1 represent the first story exterior beams and columns, respectively.

It is specified in the ASCE 7-10 that the design base shear of a structure can be reduced up to 25% when energy dissipation devices are installed. Based on this stipulation the original structure was redesigned using only 75% of the original base shear, which is 3,489 kN. Four dampers were installed in each story, one at the center bay of each exterior moment frame as shown in Fig. 25(b). The honeycomb dampers were designed in such a way that the shear capacity of the two dampers located for each direction corresponded to 25% of the story shear. The total width and height of the damper were determined to be 1,067 mm and 198 mm, respectively, and the height of each cell wall is 22 mm. The thickness of the cell wall is 3.3 mm in the third story, 4.3 mm in the second story, and 4.7 mm in the first story. The natural period of the structure decreased from 1.5 second in the structure designed with

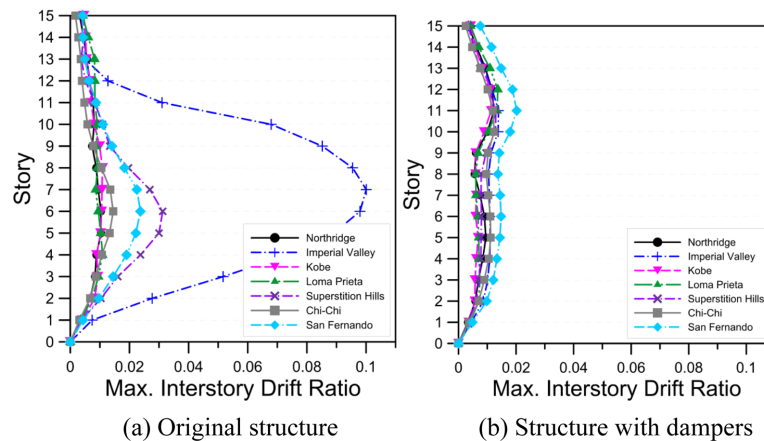


**Figure 23.** Max. inter-story drifts of the model structure subjected to seven ground motions.

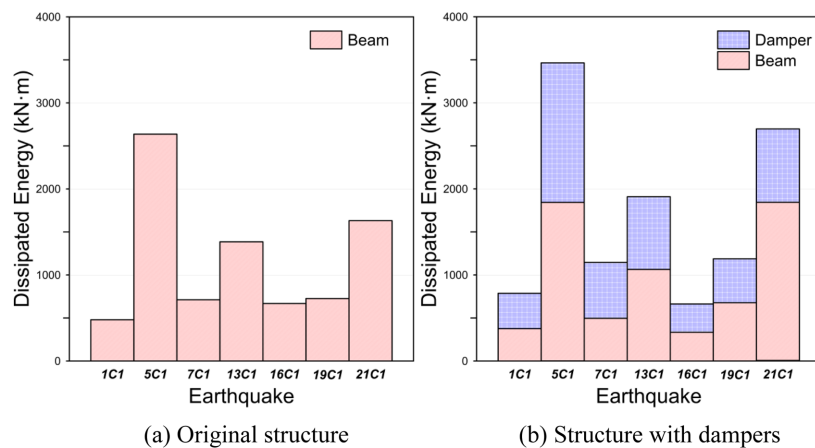
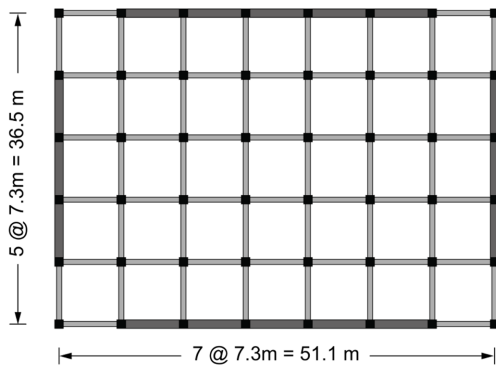
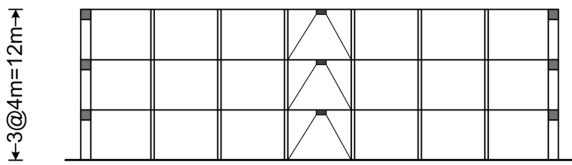


**Figure 24.** Dissipated energy in the structure during earthquakes before and after the retrofit.



(a) Structural plan



(b) Elevation of the exterior frame with honeycomb dampers

**Figure 25.** Configuration of the 3-story moment frame.

**Table 6.** Sectional properties of the 3-story structure

(a) Beams

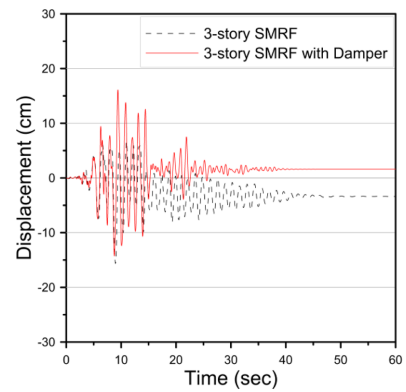
Section	Size(mm)	Rebars			
		Exterior (i,j)		Interior (m)	
		Top	Bottom	Top	Bottom
GB	460×500	3-D25	5-D25	3-D25	8-D25
SB1	460×660	9D-25	7-D25	4-D25	4-D25
SB2	460×620	10-D25	7-D25	4-D25	4-D25
SB3	460×580	7-D25	4-D25	3-D25	3-D25

(b) Columns

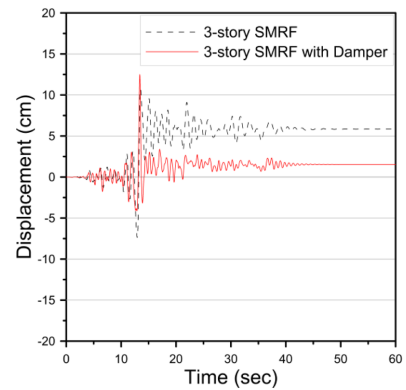
Section	Size(mm)	Rebars
GC	400×400	11-D25
SC1	680×680	16-D29
SC2	680×680	16-D29
SC3	680×680	16-D29

75% of the design base shear to 0.75 second in the structure with honeycomb dampers. It was also observed that the size of the beams and columns decreased by about 15%.

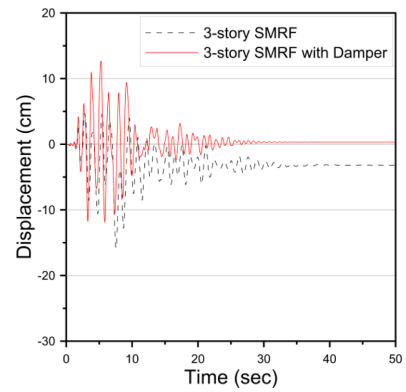
Time history analyses of the model structure with honeycomb dampers subjected to the seven selected ground motions listed in Table 5 were carried out using Perform-3D. Figure 26 shows the roof displacement time histories of the model structure designed with 100% of the design base shear and the structure designed with 75% of the base shear plus the honeycomb dampers subjected to three ground motions. It can be observed that, even though the maximum displacements turned out to be similar to each other, the structure with honeycomb



(a) Loma Prieta



(b) Superstition Hills



(c) San Fernando

**Figure 26.** Nonlinear dynamic analysis result of the 3-story moment frame.

dampers experienced less permanent displacement compared with the structure without the dampers. Figure 27 compares the maximum inter-story drifts of the two model structures obtained from dynamic analysis using the seven earthquake records. For some records the structure designed without dampers showed larger inter-story drifts, while for other records the opposite was true. Therefore no significant difference could be observed in the maximum inter-story drifts.

Figure 28 shows the dissipated hysteretic energy in the structures without and with the dampers subjected to the

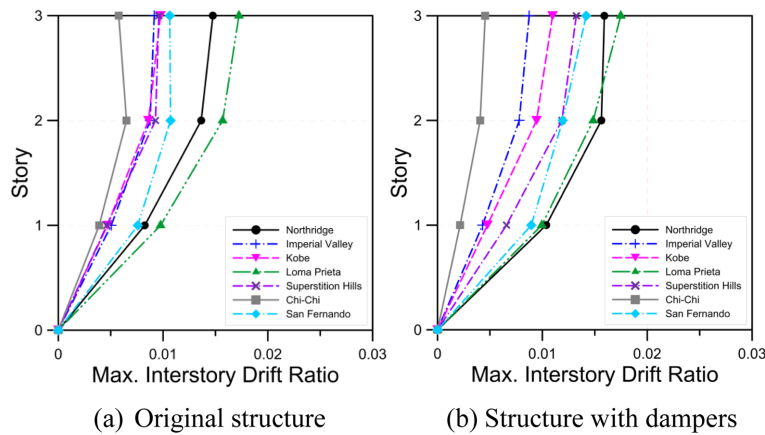


Figure 27. Maximum inter-story drift of the structure with dampers.

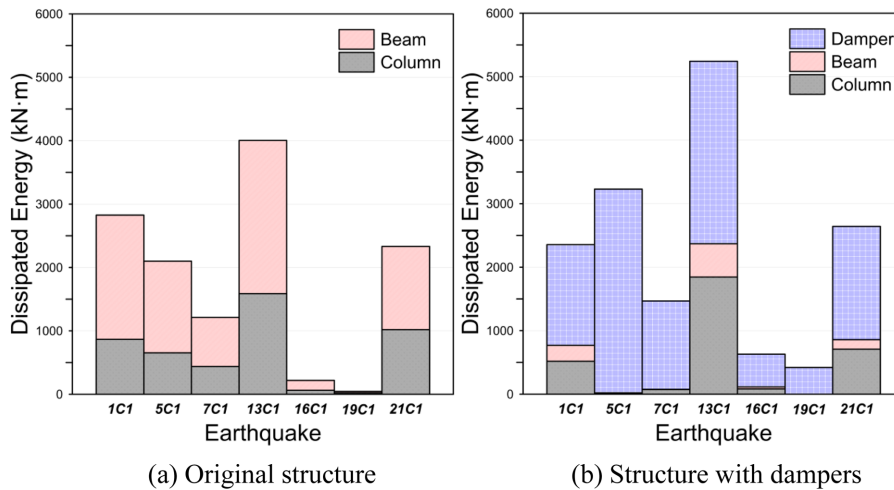


Figure 28. Dissipated inelastic energy in the model structures.

seven earthquakes. As observed in the previous example significant amount of energy was dissipated due to stable hysteretic behavior of the dampers. As a result of energy dissipation in the dampers, the energy dissipation in the structural members, especially in the beams, is quite significant.

### 6. Conclusions

This paper explored the validity of honeycomb shaped steel hysteretic dampers applied to seismic retrofit of a structure. The formulas for the initial stiffness and yield strength of a damper unit were derived based on the cell wall bending model, and the bilinear force-displacement model of the honeycomb damper was developed based on the nonlinear force-displacement relationship obtained from finite element analysis. The stiffness of the honeycomb damper turned out to be quite sensitive to the thickness to height ratio of a unit cell, and the desired stiffness, strength, and deformation capacity of a damper could easily be achieved by controlling the horizontal and vertical number

of damper units as well as the thickness/height of a unit cell.

The honeycomb dampers were applied for seismic retrofit of a 15-story RC moment frame building and for alternative seismic design of a 3-story moment frame. The analysis results of the model structures using seven earthquake records showed that the honeycomb dampers contributed significantly to the enhancement of the strength and stiffness of the model structure. The nonlinear time history analysis results showed that after installation of the dampers the permanent displacements were significantly reduced. It was also observed that in the structure with honeycomb dampers large amount of energy was dissipated in the dampers resulting in less damage in the structural members.

The main advantage of honeycomb dampers compared with other hysteretic dampers is the flexibility in the design of its configuration and yield/deformation capacities. It can be easily installed in a given space in variety of shapes. The desired stiffness and strength of the damper can easily be produced by various combinations of height, depth, thickness, and number of honeycomb cells.

## Acknowledgement

This research was supported by a grant (13AUDP-B066083-01) from Architecture & Urban Development Research Program funded by Ministry of Land, Infrastructure and Transport of Korean government

## Reference

- ABAQUS Ver. 6.9 (2009) Dassault Systmes, Simulia Corp. Providence, RI, USA.
- ACI 318-11 Building Code Requirements for Structural Concrete and Commentary, American Concrete Institute.
- Alti-Veltin B., Gandhi F. (2010) Effect of Cell Geometry on Energy Absorption of Honeycomb Under In-Plane Compression, American Institute of Aeronautics and Astronautics, pp. 466-478.
- ASCE/SEI 41-06 Seismic Rehabilitation of Existing Buildings, American Society of Civil Engineers, Reston Virginia.
- ASCE/SEI 7-10 Minimum Design Loads for Buildings and Other Structures, American Society of Civil Engineers, Reston Virginia.
- Aref A.J., Jung W.(2003) Energy-Dissipating Polymer Matrix Composite-Infill Wall System for Seismic Retrofitting, *Journal of Structural Engineering*, 129, pp. 440-448.
- Benavent Climent A., Oh S., Akiyama H.(1998) Ultimate Energy Absorption Capacity of Slit Type Steel Plates Subjected to Shear Deformations, *Journal of Structural and Construction Engineering*, AII, 503, pp. 139-147.
- Benavent Climent A., Morillas L., Vico J.M. (2010) A study on using wide-flange section web under out-of-plane flexure for passive energy dissipation, *Earthquake Engineering and Structural Dynamics*, 40, pp. 473-490.
- Chan R.W.K., Albermani F. (2008) Experimental study of steel slit damper for passive energy dissipation, *Engineering Structures*, 30, pp. 1058-1066.
- Chopra AK. Dynamics of structures: Theory and applications to earthquake engineering. Englewood Cliffs (NJ): Prentice Hall; 2007.
- Computer and Structures (2006) PERFORM components and elements for PERFORM 3D and PERFORM-Collapse ver.4, CSI, Berkeley, CA.
- Federal Emergency Management Agency (FEMA) (2007) Interim protocols for determining seismic performance characteristics of structural and nonstructural components. Report No. FEMA 461, Washington, DC, USA.
- Gibson L.J., Ashby M.F.(1997) Cellular solids Structure and Properties, 2<sup>nd</sup> ed., Cambridge University Press, Cambridge, UK.
- Ju J.,Summers J.D.(2011) Compliant Hexagonal Periodic Lattice Structures Having Both High Shear Strength and High Shear Strain, *Material and Design*, 32(2), 512-524.
- Ju J., Summers J.D., Ziegert J., George Fadel (2012) Design of Honeycombs for Modulus and Yield Strain in Shear, *Journal of Engineering Materials and Technology*, 134(1), 011002.
- Kim T., Kim J.(2007) Seismic Performance Evaluation of a RC Special Moment Frame, *Structural Engineering and Mechanics*, 27(6), pp. 671-682.
- Kobori T., Miura Y., Fukuzawa E., Yamada T., Arita T., Takenaka Y., Miyagawa N., Tanaka N., Fukumoto T. (1992) Development and application of hysteresis steel dampers, *10<sup>th</sup> World Conference of Earthquake Engineering*, Balkema, Rotterdam, pp. 2341-2346.
- Ko G., Joo J., Hwang J., Kang K. (2010) Application of Wire-woven Bulk Kagome as a Vibration Control Device for a Building Structure, *Proceedings the international Conference on Sustainable Building Asia*, pp. 293-298.
- Köken, A. and Köroğlu, M. (2015) Experimental Study on Beam-to-Column Connections of Steel Frame Structures with Steel Slit Dampers. *J. Perform. Constr. Facil.*, 29(2).
- Maleki S., Bagheri S. (2010) Pipe damper, Part I: Experimental and analytical study, *Journal of Constructional Steel Research*, 66, pp. 1088-1095.
- Maleki S., Mahjoubi S. (2013) Dual- Pipe damper, *Journal of Constructional Steel Research*, 85, pp. 81-91.
- PEER (2006) Peer NGA Database, Pacific Earthquake Engineering Research Center, University of California, Berkeley, U.S.A.
- Teruna DR, Majid TA, Budiono B (2015), Experimental Study of Hysteretic Steel Damper for Energy Dissipation Capacity, *Advances in Civil Engineering*. Published online, <http://dx.doi.org/10.1155/2015/631726>
- Tsai K., Chen H., Hong C., Su y. (1993) Design of Steel Triangular Plate Energy absorbers for Seismic-Resistant Construction, *Earthquake Spectra*, 9(3), pp. 505-528.
- Wang A.-J., McDowell D.L.(2004) In-Plane Stiffness and Yield Strength of Periodic Metal Honeycombs, *Journal of Engineering Materials and Technology*, 126, pp. 137-156.
- Whittaker A.S., Bertero V.V, Alonso L.J., Thompson C.L.(1989) Earthquake Simulator Tests of Steel Plate Added Damping and Stiffness Elements, Report No. UCB/EERC-89/02, Earthquake Engineering Research Center, University of California, Berkeley, CA.